

Quantum-Critical Spin-Density Waves in Iron-Selenide High- T_c Superconductors

Jose P. Rodriguez^{1,*}

¹*Department of Physics and Astronomy, California State University at Los Angeles, Los Angeles, California, USA*

Correspondence*:

Department of Physics and Astronomy, California State University at Los Angeles, Los Angeles, CA 90032, USA
jrodrig@calstatela.edu

ABSTRACT

Hidden spin-density waves (hSDW) with Néel ordering vector (π, π) have been proposed recently as parent groundstates to electron-doped iron-selenide superconductors. Doping such groundstates can result in visible electron-type Fermi surface pockets and faint hole-type Fermi surface pockets at the corner of the folded Brillouin zone. A Cooper pair instability that alternates in sign between the electron-type and the hole-type Fermi surfaces has recently been predicted. The previous is due to the interaction of electrons and holes with hidden spin fluctuations connected with hSDW order that is near a quantum-critical point. Quantum criticality is tuned in by increasing the strength of Hund's Rule from the hSDW state. We find that the exchange of hidden spin fluctuations by electrons/holes in the critical hSDW state results in asymptotic freedom. In particular, the strength of spin-flip interactions becomes weaker and weaker on length scales that are shorter and shorter compared to the range of hSDW order. We then argue that string states that connect well-separated particle/hole excitations in the hSDW are robust. This suggests a picture where the hole degrees of freedom mentioned previously are confined.

Keywords: superconductivity, iron superconductors, magnetism, renormalization group, asymptotic freedom, quantum criticality, spin fluctuations, spin-density waves

1 INTRODUCTION

Electron-doped iron-selenide systems show among the highest critical temperatures inside the general class of iron superconductors. A single layer of iron selenide over the appropriate substrate exhibits a critical temperature on the order of 50 K, for example[1, 2]. Unlike iron-pnictide superconductors, however, electron-doped iron selenide shows no nesting of the Fermi surfaces. Instead, angle-resolved photoemission spectroscopy (ARPES) finds evidence for electron-type Fermi surface pockets at the corner of the folded (two-iron) Brillouin zone[3, 4, 5, 6]. The hole bands that typically cross the Fermi level at the center of the Brillouin zone in iron-pnictide superconductors lie buried below the Fermi level in electron-doped iron selenide. Furthermore, ARPES and scanning tunneling microscopy (STM) find evidence for an *isotropic* quasi-particle gap that opens at the Fermi level[1, 4, 5, 6, 7, 8]. It is believed that electron-electron repulsion is moderately strong in iron superconductors generally[9, 10]. The absence of sign

changes in the gap over the Fermi surface that is observed experimentally by ARPES and by STM in electron-doped iron selenide is therefore very puzzling.

Electron-doped iron selenide also exhibits peculiarities in the nature of its low-energy spin excitations. Inelastic neutron scattering spectroscopy finds evidence for spin resonances at excitation energies that lie below the superconducting energy gap[11], but at momenta that lie mid-way between the “stripe” spin-density wave (SDW) wavevector $(\pi, 0)$ and the Néel SDW wavevector (π, π) [12, 13, 14]. Furthermore, inelastic neutron scattering spectroscopy sees a “diamond” of spin excitations centered at the wavevector (π, π) in electron-doped iron selenide[15]. The “diamond” of spin excitations notably lies at energies *above* the superconducting gap.

Upon electron doping, the author has demonstrated recently that a critical hidden spin-density wave (hSDW) state with Néel wavevector (π, π) shows electron-type Fermi surface pockets that are accompanied by vanishingly faint hole-type Fermi surface pockets at the corner of the folded (two-iron) Brillouin zone[16]. This result is consistent with those of a related local-moment model[17]. The author has also demonstrated that a Cooper pair instability exists over the electron and hole Fermi surfaces that alternates in sign between them. At half filling, the critical hSDW shows hidden magnetic order between $d+ = d_{xz} + id_{yz}$ and $d- = d_{xz} - id_{yz}$ orbitals[18]. (See Fig. 2a.) Lowering the strength of Hund’s Rule coupling tunes the critical hSDW into the hidden order phase[19, 20]. The author has also demonstrated that the hSDW shows “rings” and “diamonds” of low-energy spin excitations around the Néel wave vector (π, π) [18, 21]. Such low-energy spin excitations collapse to zero energy at the critical hSDW.

The electron-doped hSDW described above is a promising candidate groundstate for electron-doped iron-selenide high-temperature superconductors. It is predicted to be an S^{+-} -wave superconductor, with Cooper pairs that alternate in sign between visible electron Fermi surface pockets and faint hole Fermi surface pockets at the corner of the folded (two-iron) Brillouin zone[16]. It is controlled, however, by the critical hSDW at half filling. (See Fig. 3b.) Related critical hSDW states have been studied previously in the context of copper-oxide high-temperature superconductors[22]. (See Fig. 2c.) They are notably free of the sign problem in quantum Monte Carlo simulations. In this paper, we shall continue to scrutinize the critical hSDW at half filling via an Eliashberg Theory analysis in the particle-hole channel[18]. Here, electrons and holes interact with hidden spinwaves that result from long-range hSDW order. The spinwaves disperse acoustically from the Néel wavevector (π, π) . A renormalization group is discovered that is based on the correction to the interaction vertex. It predicts asymptotic freedom[23, 24, 25, 26]: spin-flip interactions become weaker and weaker at shorter and shorter length scales compared to the range of hSDW order. At the opposite extreme, we argue that this is related to confining *string* states between well-separated electron/hole excitations[27, 28, 29]. (See Fig. 6.)

2 NESTED FERMI SURFACES AND HIDDEN SPIN-DENSITY WAVE

An extended Hubbard model for a single layer of electron-doped iron selenide is introduced below. Mean field theory will reveal that it harbors hidden magnetic order[18].

2.1 Extended Hubbard Model

We retain only the $3d_{xz}/3d_{yz}$ orbitals of the iron atoms in the following description of a single layer of heavily electron-doped FeSe. In particular, let us work in the isotropic basis of orbitals $d- = (d_{xz} - id_{yz})/\sqrt{2}$ and $d+ = (d_{xz} + id_{yz})/\sqrt{2}$. Electrons hop among the $d+$ and $d-$ orbitals between nearest neighbors (1) and next-nearest neighbors (2) on the square lattice of iron atoms that make up a single

layer of FeSe. The kinetic energy due to hopping over the square lattice of iron atoms is then governed by the following Hamiltonian expressed in momentum space:

$$H_{\text{hop}} = \sum_{\mathbf{k}} \sum_{\alpha} \sum_s \varepsilon_{\parallel}(\mathbf{k}) c_{\alpha,s}^{\dagger}(\mathbf{k}) c_{\alpha,s}(\mathbf{k}) + \sum_{\mathbf{k}} \sum_s [\varepsilon_{\perp}(\mathbf{k}) c_{d+,s}^{\dagger}(\mathbf{k}) c_{d-,s}(\mathbf{k}) + \text{h.c.}], \quad (1)$$

where

$$\varepsilon_{\parallel}(\mathbf{k}) = -2t_1^{\parallel}(\cos k_x a + \cos k_y a) - 2t_2^{\parallel}(\cos k_+ a + \cos k_- a) \quad (2a)$$

$$\varepsilon_{\perp}(\mathbf{k}) = -2t_1^{\perp}(\cos k_x a - \cos k_y a) - 2t_2^{\perp}(\cos k_+ a - \cos k_- a) \quad (2b)$$

are intra-orbital and inter-orbital matrix elements, with $k_{\pm} = k_x \pm k_y$. Above also, $c_{\alpha,s}(\mathbf{k})$ and $c_{\alpha,s}^{\dagger}(\mathbf{k})$ denote operators that destroy and create an electron of spin s in orbital α , and with momentum $\hbar\mathbf{k}$. The reflection symmetries shown by a single layer of FeSe imply that the intra-orbital (\parallel) and inter-orbital (\perp) hopping matrix elements of the Hamiltonian (1) show s -wave and d -wave symmetry, respectively[30, 31, 32]. The momentum dependence of the intra-orbital (2a) and inter-orbital (2b) matrix elements $\varepsilon_{\parallel}(\mathbf{k})$ and $\varepsilon_{\perp}(\mathbf{k})$ display those symmetries. Here, the nearest neighbor intra-orbital and inter-orbital hopping matrix elements t_1^{\parallel} and t_1^{\perp} are real, the next-nearest neighbor intra-orbital hopping matrix element t_2^{\parallel} is also real, and the next-nearest neighbor inter-orbital hopping matrix element t_2^{\perp} is pure imaginary.

The hopping Hamiltonian (1) is easily diagonalized[18] by plane waves of $d_{x(\delta)z}$ and $id_{y(\delta)z}$ orbitals that are rotated with respect to the principal axis by a phase shift δ that depends on momentum. They are created by the corresponding operators:

$$\begin{aligned} c_s^{\dagger}(2, \mathbf{k}) &= 2^{-1/2} [e^{-i\delta(\mathbf{k})} c_{d-,s}^{\dagger}(\mathbf{k}) + e^{+i\delta(\mathbf{k})} c_{d+,s}^{\dagger}(\mathbf{k})], \\ c_s^{\dagger}(1, \mathbf{k}) &= 2^{-1/2} [e^{-i\delta(\mathbf{k})} c_{d-,s}^{\dagger}(\mathbf{k}) - e^{+i\delta(\mathbf{k})} c_{d+,s}^{\dagger}(\mathbf{k})]. \end{aligned} \quad (3)$$

The phase shift $\delta(\mathbf{k})$ is set by $\varepsilon_{\perp}(\mathbf{k}) = |\varepsilon_{\perp}(\mathbf{k})| e^{i2\delta(\mathbf{k})}$. Specifically,

$$\cos 2\delta(\mathbf{k}) = \frac{-t_1^{\perp}(\cos k_x a - \cos k_y a)}{\sqrt{t_1^{\perp 2}(\cos k_x a - \cos k_y a)^2 + |2t_2^{\perp}|^2(\sin k_x a)^2(\sin k_y a)^2}}, \quad (4a)$$

$$\sin 2\delta(\mathbf{k}) = \frac{2(t_2^{\perp}/i)(\sin k_x a)(\sin k_y a)}{\sqrt{t_1^{\perp 2}(\cos k_x a - \cos k_y a)^2 + |2t_2^{\perp}|^2(\sin k_x a)^2(\sin k_y a)^2}}. \quad (4b)$$

It is notably singular at $\mathbf{k} = 0$ and \mathbf{Q}_{AF} , where the matrix element $\varepsilon_{\perp}(\mathbf{k})$ vanishes. The energy eigenvalues of the bonding ($n = 2$) and the anti-bonding ($n = 1$) states are respectively then given by $\varepsilon_+(\mathbf{k}) = \varepsilon_{\parallel}(\mathbf{k}) + |\varepsilon_{\perp}(\mathbf{k})|$ and $\varepsilon_-(\mathbf{k}) = \varepsilon_{\parallel}(\mathbf{k}) - |\varepsilon_{\perp}(\mathbf{k})|$.

If we now turn off next-nearest neighbor intra-orbital hopping, $t_2^{\parallel} = 0$, the above energy bands then satisfy the perfect nesting condition[18],

$$\varepsilon_{\pm}(\mathbf{k} + \mathbf{Q}_{\text{AF}}) = -\varepsilon_{\mp}(\mathbf{k}). \quad (5)$$

Here $\mathbf{Q}_{\text{AF}} = (\pi/a, \pi/a)$ is the checkerboard ordering vector on the square lattice of iron atoms. As a result, the Fermi level lies at $\epsilon_F = 0$ at half filling. Figure 1 shows such perfectly nested electron-type and

hole-type Fermi surfaces for hopping parameters $t_1^{\parallel} = 100$ meV, $t_1^{\perp} = 500$ meV, $t_2^{\parallel} = 0$ and $t_2^{\perp} = 100i$ meV. It also displays the density of states of the bonding band, $n = 2$. The step at 0.4 eV and the sharp peak near 0.5 eV mark where constant-energy contours in momentum space experience a change in topology. Such transitions will play an important role below.

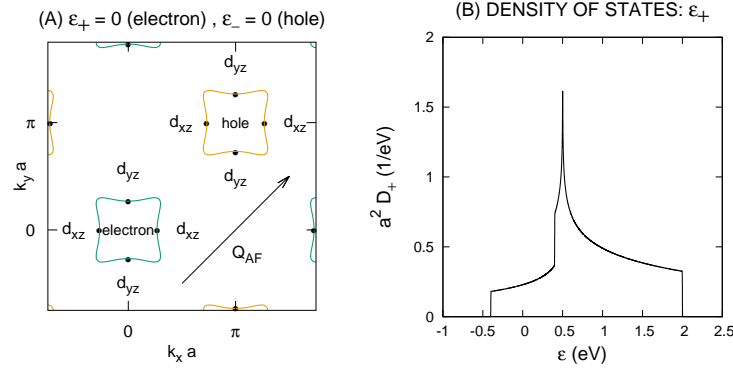


Figure 1. (a) Perfectly nested Fermi surfaces at half filling: $\epsilon_+(\mathbf{k}) = 0$ and $\epsilon_-(\mathbf{k}) = 0$, with hopping matrix elements $t_1^{\parallel} = 100$ meV, $t_1^{\perp} = 500$ meV, $t_2^{\parallel} = 0$, and $t_2^{\perp} = 100i$ meV. (See Fig. 5 for the band structure.) Dirac cones emanate from the dots on each Fermi surface. (b) Also displayed is the density of states of the bonding band, $\epsilon_+(\mathbf{k})$.

The principal interactions among the electrons are on-site ones due to Coulomb repulsion. They have four parts that are included in the following extended Hubbard model for the interaction Hamiltonian[33]:

$$H_U = \sum_i [U_0 \sum_{\alpha} n_{i,\alpha,\uparrow} n_{i,\alpha,\downarrow} + J_0 \mathbf{S}_{i,d-} \cdot \mathbf{S}_{i,d+} + U'_0 n_{i,d+} n_{i,d-} + J'_0 (c_{i,d+, \uparrow}^\dagger c_{i,d+, \downarrow}^\dagger c_{i,d-, \downarrow} c_{i,d-, \uparrow} + \text{h.c.})]. \quad (6)$$

Here, $n_{i,\alpha,s} = c_{i,\alpha,s}^\dagger c_{i,\alpha,s}$ is the occupation operator and $\mathbf{S}_{i,\alpha} = \frac{1}{2} \sum_{s,s'} c_{i,\alpha,s}^\dagger \boldsymbol{\sigma}_{s,s'} c_{i,\alpha,s'}$ is the spin operator, while $n_{i,\alpha} = n_{i,\alpha,\uparrow} + n_{i,\alpha,\downarrow}$. Above also, $U_0 > 0$ denotes the intra-orbital on-site Coulomb repulsion energy, while $U'_0 > 0$ denotes the inter-orbital one. Last, $J_0 < 0$ is the Hund's Rule exchange coupling constant, which is ferromagnetic, while J'_0 denotes the matrix element for on-site Josephson tunneling between orbitals.

We shall also include super-exchange interactions among magnetic moments of neighboring iron atoms via the Se atoms[34, 35]:

$$H_{\text{sprx}} = \sum_{\langle i,j \rangle} J_1 (\mathbf{S}_{i,d-} + \mathbf{S}_{i,d+}) \cdot (\mathbf{S}_{j,d-} + \mathbf{S}_{j,d+}) + \sum_{\langle\langle i,j \rangle\rangle} J_2 (\mathbf{S}_{i,d-} + \mathbf{S}_{i,d+}) \cdot (\mathbf{S}_{j,d-} + \mathbf{S}_{j,d+}). \quad (7)$$

Above, J_1 and J_2 are positive super-exchange coupling constants over nearest neighbor and next-nearest neighbor iron sites. Magnetic frustration shall be assumed, henceforth, to be moderate to strong: $J_2 > 0.5J_1$,

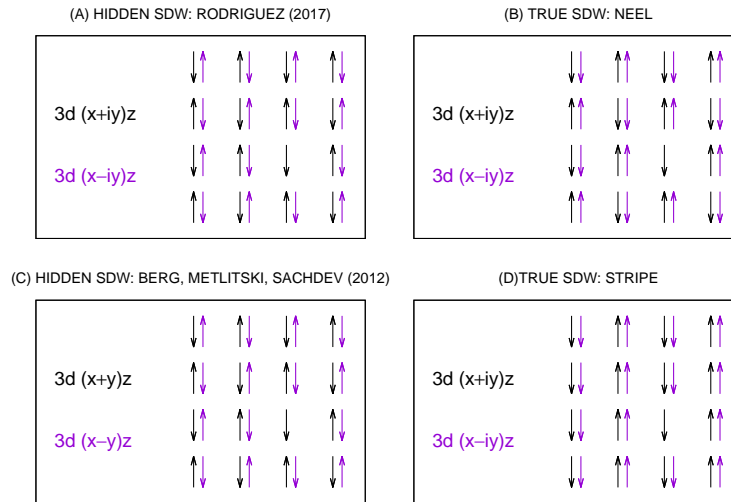


Figure 2. Hidden spin-density waves versus true spin-density waves.

2.2 Mean Field Theory

The perfect nesting of the Fermi surfaces shown by Fig. 1 implies a spin-density wave groundstate for the extended Hubbard model at half filling[18]. Possible groundstates are the hSDW state and the true SDW state displayed by Figs. 2a and 2b. Recent RPA calculations about the hSDW state confirm that magnetic frustration in H_{sprx} (7) suppresses conventional Néel order among the iron moments in favor of hSDW order[21]. A mean field theory for the hSDW state of the extended Hubbard model described above can be developed along the lines of the mean field theory for the SDW state of the conventional one-orbital Hubbard model over the square lattice[36]. In particular, assume that the magnetic moment per site per orbital is hidden, with spontaneous symmetry breaking along the z axis, and that it flips sign in a checkerboard fashion across the square lattice of iron atoms:

$$\langle m_{i,\alpha} \rangle = (-1)^\alpha e^{i\mathbf{Q}_{\text{AF}} \cdot \mathbf{r}_i} \langle m_{0,0} \rangle, \quad (8)$$

where $\langle m_{i,\alpha} \rangle = \frac{1}{2} \langle n_{i,\alpha,\uparrow} \rangle - \frac{1}{2} \langle n_{i,\alpha,\downarrow} \rangle$. Here, the $d-$ and $d+$ orbitals are indexed by $\alpha = 0$ and 1. It is important to notice that this hSDW state is notably invariant under rotations of the $3d_{xz}$ and $3d_{yz}$ orbitals about the z axis. It therefore cannot show any tendency towards nematic order[37, 38]. A standard mean-field replacement of the intra-orbital on-site interactions (U_0) and of the Hund's Rule coupling (J_0) yields the contribution to the electronic energy[18]

$$- \sum_i \sum_\alpha U(\pi) \langle m_{i,\alpha} \rangle (n_{i,\alpha,\uparrow} - n_{i,\alpha,\downarrow}) = - \langle m_{0,0} \rangle U(\pi) \sum_i \sum_\alpha (-1)^\alpha e^{i\mathbf{Q}_{\text{AF}} \cdot \mathbf{r}_i} (n_{i,\alpha,\uparrow} - n_{i,\alpha,\downarrow}), \quad (9)$$

where

$$U(\pi) = U_0 + \frac{1}{2} J_0. \quad (10)$$

A similar mean-field replacement of the inter-orbital on-site interactions (U'_0) leads entirely to a shift of the chemical potential[18]. Also, no net magnetic moment exists on each iron site within mean field theory because of hidden magnetic order. Hence, the super-exchange Hamiltonian (7) makes no contribution within mean field theory as well. Last, notice that on-site Josephson tunneling between orbitals (J'_0) in H_U is suppressed at strong on-site-orbital repulsion, U_0 . We shall henceforth neglect this contribution to the extended Hubbard model (6) on that basis.

Inverting the planewaves (3) to site-orbital space yields expressions for the corresponding creation operators:

$$\begin{aligned} c_{i,d-,s}^\dagger &= \mathcal{N}^{-1/2} \sum_{\mathbf{k}} e^{-i\mathbf{k}\cdot\mathbf{r}_i} e^{+i\delta(\mathbf{k})} [c_s^\dagger(2, \mathbf{k}) + c_s^\dagger(1, \mathbf{k})], \\ c_{i,d+,s}^\dagger &= \mathcal{N}^{-1/2} \sum_{\mathbf{k}} e^{-i\mathbf{k}\cdot\mathbf{r}_i} e^{-i\delta(\mathbf{k})} [c_s^\dagger(2, \mathbf{k}) - c_s^\dagger(1, \mathbf{k})]. \end{aligned} \quad (11)$$

Here $\mathcal{N} = 2N_{\text{Fe}}$ is the number of iron site-orbitals. Substitution of expressions (11) and their conjugates into the right-hand side of the mean-field approximation for the interaction energy (9) ultimately yields a mean-field Hamiltonian of the form

$$\begin{aligned} H^{(mf)} &= \sum_s \sum_{\mathbf{k}} \varepsilon_+(\mathbf{k}) [c_s^\dagger(2, \mathbf{k}) c_s(2, \mathbf{k}) - c_s^\dagger(1, \bar{\mathbf{k}}) c_s(1, \bar{\mathbf{k}})] \\ &\quad + \sum_s \sum_{\mathbf{k}} [(\text{sgn } s) \Delta(\mathbf{k}) c_s^\dagger(1, \bar{\mathbf{k}}) c_s(2, \mathbf{k}) + \text{h.c.}], \end{aligned} \quad (12)$$

where $\bar{\mathbf{k}} = \mathbf{k} + \mathbf{Q}_{\text{AF}}$. The gap function is anisotropic, and it depends on momentum as

$$\Delta(\mathbf{k}) = \Delta_0 \sin[2\delta(\mathbf{k})], \quad (13)$$

with

$$\Delta_0 = \langle m_{0,0} \rangle U(\pi). \quad (14)$$

Above, we have shifted the momentum of the anti-bonding band ($n = 1$) by \mathbf{Q}_{AF} , and we have subsequently exploited the perfect-nesting condition (5). Above, also, intra-band scattering has been neglected because it shows no nesting.

Inspection of the mean-field Hamiltonian (12) yields that it has energy eigenvalues equal to plus or minus $E(\mathbf{k}) = [\varepsilon_+^2(\mathbf{k}) + \Delta^2(\mathbf{k})]^{1/2}$. By (4b), the gap function (13) shows nodes along the principal axes. Dirac cones therefore emanate from the four points where the Fermi surfaces, $\varepsilon_+(\mathbf{k}) = 0$ and $\varepsilon_-(\mathbf{k}) = 0$, cross the principal axes. These points are displayed by Fig. 1a. The new one-electron energy spectrum, $\pm E(\mathbf{k})$, is due to resonant scattering of bonding and anti-bonding planewaves (3) by the underlying hSDW, which breaks the translational symmetry of the square lattice of iron atoms. Amplitudes for the bonding (+) and for the anti-bonding (−) components of the new mixed eigenstates are given by the standard *coherence factors*. A *gap equation* for the gap maximum (14) can be thereby obtained, which yields the ordered hSDW moment, $\langle m_{0,0} \rangle$, as a function of the hopping parameters and of $U(\pi)$. (See ref. [18].) Surprisingly, by (10), such mean-field solutions remain valid for any pair of on-site-orbital repulsion and Hund's Rule coupling, U_0 and $-J_0$, such that $U(\pi)$ remains constant. Figure 3a displays that degeneracy.

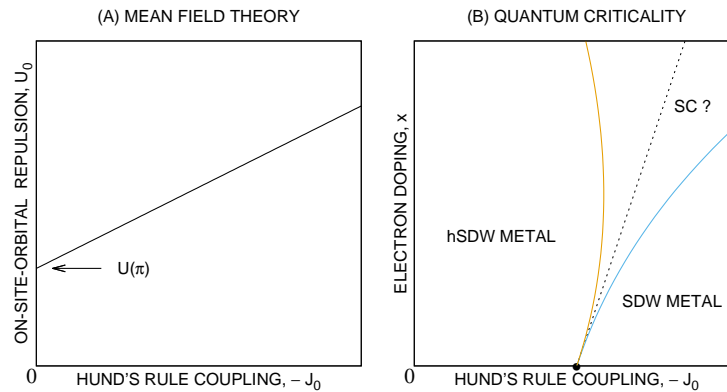


Figure 3. (a) Absent quantum critical point (QCP) within mean field theory versus (b) QCP, at constant interaction strength, $U(\pi)$, as Hund's Rule is enforced.

3 QUANTUM FIELD THEORY AT CRITICALITY

The hSDW introduced above must clearly become unstable above a threshold strength in Hund's Rule, $-J_{0c}$. This fact is not captured by the previous mean field theory. (See Fig. 3.) Indeed, the Heisenberg model predicts that the stripe SDW (Fig. 2d) intervenes above a threshold strength in Hund's Rule [19, 20]. Also, a recent RPA calculation of the present extended Hubbard model is compatible with the Néel SDW (Fig. 2b) intervening above a threshold Hund's Rule coupling instead [21]. Below, we will include fluctuations of the hSDW order parameter, which will permit a proper description of the critical hSDW state that exists at $\Delta_0 \rightarrow 0$.

3.1 Hidden Spinwaves, Interaction with Electrons

Like in the previous mean field theory, let us start from the ordered hSDW state (8). Assume, in particular, a long-range ordered moment that alternates in sign between the $d+$ and $d-$ orbitals, and between nearest neighbor iron sites on the square lattice. Basic considerations imply Goldstone modes in the transverse directions, $m_x(\pi)$ and $m_y(\pi)$, at the checkerboard wave number, $\mathbf{Q}_{AF} = (\pi/a, \pi/a)$, where $\mathbf{m}(\pi) = \mathbf{m}_{d-} - \mathbf{m}_{d+}$ is the hidden magnetic moment [18]. Specifically, the spin-flip propagator, $iD(\mathbf{q}, \omega) = \langle \frac{1}{\sqrt{2}} m^+(\pi) \frac{1}{\sqrt{2}} m^-(\pi) \rangle_{\mathbf{q}, \omega}$, has the hydrodynamic form

$$D(\mathbf{q}, \omega) = \frac{(2s_1)^2}{\chi_{\perp}} [\omega^2 - \omega_b^2(\mathbf{q})]^{-1} \quad (15)$$

in the long wave length limit. Here, $m^{\pm}(\pi) = m_x(\pi) \pm i m_y(\pi)$. The propagator above shows a pole in frequency that disperses acoustically as $\omega_b(\bar{\mathbf{q}}) = c_0 |\bar{\mathbf{q}}|$, where $\bar{\mathbf{q}} = \mathbf{q} + \mathbf{Q}_{AF}$, and where c_0 is the hidden-spin-wave velocity. Above, s_1 is the ordered hSDW moment per orbital. Last, χ_{\perp} is the transverse spin susceptibility of the hidden Néel state. This form for the spin-flip propagator (15) is required by standard antiferromagnetic dynamics [39, 40, 41]. Recent RPA calculations of the hSDW state reveal such hidden Goldstone modes that disperse acoustically [21].

The above hidden spinwaves interact with electrons via the intra-orbital Hubbard interaction (U_0) and the Hund's Rule coupling (J_0) following $-\sum_i \sum_\alpha U(\pi) \mathbf{m}_{i,\alpha} \cdot 2\mathbf{S}_{i,\alpha}$. This form is suggested by mean field theory (9), in which case the super-exchange interaction (7) makes no contribution in the hSDW state. Again, on-site Josephson tunneling (J'_0) is neglected on the basis that on-site-orbital repulsion U_0 is strong enough to suppress the formation of on-site-orbital singlets. Keeping only the dominant transverse excitations then yields the interaction $-\sum_i \sum_\alpha U(\pi)(m_{i,\alpha}^+ S_{i,\alpha}^- + m_{i,\alpha}^- S_{i,\alpha}^+)$. Plugging in the transforms (11) between real space and momentum space yields ultimately the following form of the interaction between hidden spinwaves and electrons[18]:

$$H_{e\text{-hsw}} = +\frac{1}{\sqrt{2}} \frac{U(\pi)}{a\mathcal{N}^{1/2}} \sum_{\mathbf{k}} \sum_{\mathbf{k}'} [m^+(\pi, \mathbf{q}) C_{\downarrow}^\dagger(\mathbf{k}') \tau_1 C_{\uparrow}(\mathbf{k}) \sin[\delta(\mathbf{k}) + \delta(\mathbf{k}')] + \text{h.c.}], \quad (16)$$

where $\mathbf{q} = \mathbf{k} - \bar{\mathbf{k}}'$ is the momentum transfer. Here, we have introduced Nambu-Gorkov spinors[42, 43],

$$C_s(\mathbf{k}) = \begin{bmatrix} c_s(2, \mathbf{k}) \\ c_s(1, \bar{\mathbf{k}}) \end{bmatrix}, \quad (17)$$

which explicitly account for perfect nesting of the Fermi surfaces. Also, τ_1 is the Pauli matrix along the x axis. Last, intra-band scattering has been neglected because it shows no nesting.

3.2 Self-Energy Correction and Eliashberg Equations

We shall now compute the electron propagators within a self-consistent approximation. They are defined by the 2×2 matrix $iG_s(\mathbf{k}, \omega) = \int dt_{1,2} e^{i\omega t_{1,2}} \langle T[C_s(\mathbf{k}, t_1) C_s^\dagger(\mathbf{k}, t_2)] \rangle$, where $t_{1,2} = t_1 - t_2$, and where T is the time-ordering operator. Here, $C_s(\mathbf{k}, t)$ and $C_s^\dagger(\mathbf{k}, t)$ are the time evolutions of the respective destruction and creation operators, $C_s(\mathbf{k})$ and $C_s^\dagger(\mathbf{k})$. In the absence of interactions, $U(\pi) \rightarrow 0$, perfect nesting (5) yields that the matrix inverse of the electron propagator is given by

$$G_0^{-1}(\mathbf{k}, \omega) = \omega \tau_0 - \varepsilon_+(\mathbf{k}) \tau_3, \quad (18)$$

where τ_0 is the 2×2 identity matrix, and where τ_3 is the Pauli matrix along the z axis. Inspection of the mean-field Hamiltonian (12) suggests, on the other hand, the following form for the matrix inverse of the exact electron propagator:

$$G_s^{-1}(\mathbf{k}, \omega) = Z(\mathbf{k}, \omega) \omega \tau_0 - [\varepsilon_+(\mathbf{k}) - \nu] \tau_3 - (\text{sgn } s) Z(\mathbf{k}, \omega) \Delta(\mathbf{k}) \tau_1. \quad (19)$$

Here, $Z(\mathbf{k}, \omega)$ is the wavefunction renormalization, $\Delta(\mathbf{k})$ is the quasi-particle gap (13), and ν is a relative energy shift of the bands that preserves perfect nesting. Comparison of (18) and (19) then yields the self-energy correction

$$\Sigma_s(\mathbf{k}, \omega) = [1 - Z(\mathbf{k}, \omega)] \omega \tau_0 - \nu \tau_3 + (\text{sgn } s) Z(\mathbf{k}, \omega) \Delta(\mathbf{k}) \tau_1 \quad (20)$$

to the band dispersions $\varepsilon_+(\mathbf{k}) \tau_3$.

The self-consistent approximation for the electron propagator is displayed by Fig. 4a. The self-energy correction (20) is thereby approximated by

$$\Sigma_s(\mathbf{k}, \omega) = i \int_{\text{BZ}} \frac{d^2 k'}{(2\pi)^2} \int_{-\infty}^{+\infty} \frac{d\omega'}{2\pi} \frac{U^2(\pi)}{2} \sin^2[\delta(\mathbf{k}) + \delta(\mathbf{k}')] D(\mathbf{q}, q_0) \tau_1 G_{\bar{s}}(\mathbf{k}', \omega') \tau_1, \quad (21)$$

with $q_0 = \omega - \omega'$, and with $\mathbf{q} = \mathbf{k} - \bar{\mathbf{k}}'$. Now write the electron propagator in terms of components of Pauli matrices, τ_μ : $G = \sum_{\mu=0}^3 G^{(\mu)} \tau_\mu$. This yields the corresponding components for the self-energy correction:

$$\Sigma_s^{(\mu)}(\mathbf{k}, \omega) = \text{sgn}_\mu(1) \int_{\text{BZ}} \frac{d^2 k'}{(2\pi)^2} \frac{U^2(\pi)}{2} \sin^2[\delta(\mathbf{k}) + \delta(\mathbf{k}')] i \int_{-\infty}^{+\infty} \frac{d\omega'}{2\pi} D(\mathbf{q}, q_0) G_s^{(\mu)}(\mathbf{k}', \omega'). \quad (22)$$

Here, we have used the identity satisfied by Pauli matrices, $\tau_1 \tau_\mu \tau_1 = \text{sgn}_\mu(1) \tau_\mu$, where $\text{sgn}_0(1) = +1 = \text{sgn}_1(1)$, and where $\text{sgn}_2(1) = -1 = \text{sgn}_3(1)$. Now recall that the components $G^{(\mu)}$ of the matrix inverse of (19) are given explicitly by

$$\begin{aligned} G_s^{(0)} &= \frac{1}{2Z} \left(\frac{1}{\omega - E + i\eta} + \frac{1}{\omega + E - i\eta} \right), \\ G_s^{(1)} &= \frac{1}{2Z} \left(\frac{1}{\omega - E + i\eta} - \frac{1}{\omega + E - i\eta} \right) \frac{\Delta}{E} (\text{sgn } s), \\ G_s^{(2)} &= 0, \\ G_s^{(3)} &= \frac{1}{2Z} \left(\frac{1}{\omega - E + i\eta} - \frac{1}{\omega + E - i\eta} \right) \frac{(\varepsilon_+ - \nu)}{ZE}, \end{aligned} \quad (23)$$

with excitation energy

$$E(\mathbf{k}, \omega) = \sqrt{\left[\frac{\varepsilon_+(\mathbf{k}) - \nu}{Z(\mathbf{k}, \omega)} \right]^2 + \Delta^2(\mathbf{k})}. \quad (24)$$

Here, $\eta \rightarrow 0+$. Next, it is useful to write the propagator for hidden spinwaves (15) as

$$D(\mathbf{q}, \omega) = \frac{(2s_1)^2}{\chi_\perp} \frac{1}{2\omega_b(\mathbf{q})} \left[\frac{1}{\omega - \omega_b(\mathbf{q}) + i\eta} - \frac{1}{\omega + \omega_b(\mathbf{q}) - i\eta} \right]. \quad (25)$$

The frequency integrals in expressions (22) for the self energies can be evaluated by going into the complex plane, and by exploiting Cauchy's residue theorem in the standard way. The result amounts to Brillouin-Wigner second-order perturbation theory[44, 45]. In particular, comparison with the form (20) of the

self-energy correction yields the following Eliashberg equations at zero temperature[18]:

$$[Z(\mathbf{k}, \omega) - 1]\omega = \int_{\text{BZ}} \frac{d^2 k'}{(2\pi)^2} U^2(\pi) \frac{s_1^2 \sin^2[\delta(\mathbf{k}) + \delta(\mathbf{k}')] }{\chi_\perp Z(\mathbf{k}', \omega')} \cdot \frac{1}{2\omega_b(\mathbf{q})} \left[\frac{1}{\omega_b(\mathbf{q}) + E(\mathbf{k}') - \omega} - \frac{1}{\omega_b(\mathbf{q}) + E(\mathbf{k}') + \omega} \right], \quad (26a)$$

$$-\nu = \int_{\text{BZ}} \frac{d^2 k'}{(2\pi)^2} U^2(\pi) \frac{s_1^2 \sin^2[\delta(\mathbf{k}) + \delta(\mathbf{k}')] }{\chi_\perp Z(\mathbf{k}', \omega')} \frac{\varepsilon_+(\mathbf{k}') - \nu}{Z(\mathbf{k}', \omega') E(\mathbf{k}')} \cdot \frac{1}{2\omega_b(\mathbf{q})} \left[\frac{1}{\omega_b(\mathbf{q}) + E(\mathbf{k}') - \omega} + \frac{1}{\omega_b(\mathbf{q}) + E(\mathbf{k}') + \omega} \right], \quad (26b)$$

$$Z(\mathbf{k}, \omega)\Delta(\mathbf{k}) = \int_{\text{BZ}} \frac{d^2 k'}{(2\pi)^2} U^2(\pi) \frac{s_1^2 \sin^2[\delta(\mathbf{k}) + \delta(\mathbf{k}')] }{\chi_\perp Z(\mathbf{k}', \omega')} \frac{\Delta(\mathbf{k}')}{E(\mathbf{k}')} \cdot \frac{1}{2\omega_b(\mathbf{q})} \left[\frac{1}{\omega_b(\mathbf{q}) + E(\mathbf{k}') - \omega} + \frac{1}{\omega_b(\mathbf{q}) + E(\mathbf{k}') + \omega} \right], \quad (26c)$$

where $\omega' = E(\mathbf{k}')$. Below, we shall find a solution to these equations that describes a quantum-critical hSDW at $Z(\mathbf{k}, \omega)\Delta(\mathbf{k}) \rightarrow 0$.

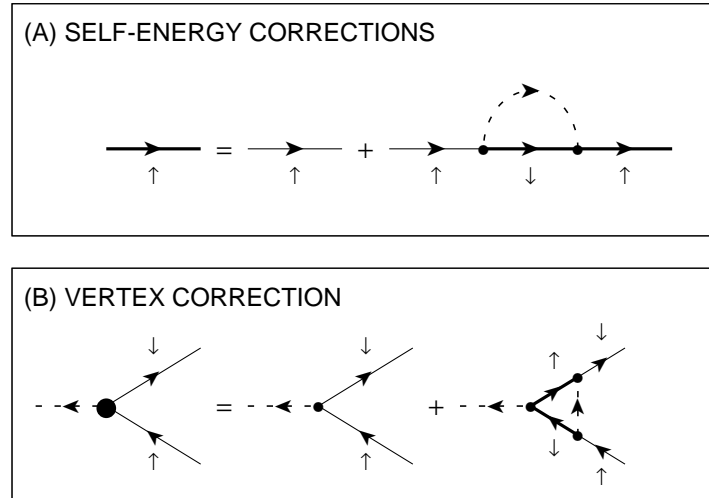


Figure 4. Feynman diagrams (a) for the Eliashberg equations and (b) for the second-order vertex correction to the interaction, Eqs. (16) and (17). Thin and thick solid lines represent, respectively, the bare and the “dressed” electron propagators, G_0 and G_s , while dashed lines represent the spin-flip propagator, D .

3.3 Quantum-Critical hSDW, Lifshitz Transition

The author and Melendrez have shown that a quantum-critical hSDW solution of the Eliashberg equations (26a)-(26c) exists at[18] $Z(\mathbf{k}, \omega)\Delta(\mathbf{k}) \rightarrow 0$. Isotropy of the excitation energy $E(\mathbf{k}')$ over the Fermi surface is restored in such case. Like conventional Eliashberg theory for S -wave superconductors, it then becomes convenient to replace the integrals over momentum in (26a) and (26b) by integrals over

$\varepsilon' = \varepsilon_+(\mathbf{k}')$ and $\Omega = \omega_b(\mathbf{q})$. The previous Eliashberg equations (26a) and (26b) thereby reduce to [18]

$$(Z - 1)\omega = \int_{-W_{\text{bottom}}}^{+W_{\text{top}}} d\varepsilon' Z^{-1} \int_0^{\omega_{\text{uv}}} d\Omega \frac{\epsilon_E(\nu)}{\Omega} \cdot \frac{1}{2} \left[\frac{1}{\Omega + |\varepsilon' - \nu|/Z - \omega} - \frac{1}{\Omega + |\varepsilon' - \nu|/Z + \omega} \right], \quad (27a)$$

$$-\nu = \int_{-W_{\text{bottom}}}^{+W_{\text{top}}} d\varepsilon' Z^{-1} \int_0^{\omega_{\text{uv}}} d\Omega \frac{\epsilon_E(\nu)}{\Omega} \frac{\varepsilon' - \nu}{|\varepsilon' - \nu|} \cdot \frac{1}{2} \left[\frac{1}{\Omega + |\varepsilon' - \nu|/Z - \omega} + \frac{1}{\Omega + |\varepsilon' - \nu|/Z + \omega} \right], \quad (27b)$$

where ω_{uv} is an ultra-violet frequency cutoff for hidden spinwaves, and where $[-W_{\text{bottom}}, +W_{\text{top}}]$ is the range of the energy band $\varepsilon_+(\mathbf{k})$. (See Fig. 1b.) Above, we have introduced the Eliashberg energy scale [18]

$$\epsilon_E(\nu) = \frac{1}{D_+(\nu)} \oint_{\text{FS}_+} \frac{dk_{\parallel}}{(2\pi)^4} U^2(\pi) \frac{s_1^2}{\chi_{\perp}} \frac{[\sin 2\delta(\mathbf{k})]^2}{c_0 |\mathbf{v}_+(\mathbf{k})|^2}, \quad (28)$$

where FS_+ denotes the Fermi surface $\varepsilon_+(\mathbf{k}) = \nu$, where $D_+(\nu)$ is the density of states of the $n = 2$ bonding band shown by Fig. 1b, and where c_0 is the velocity of hidden spinwaves at \mathbf{Q}_{AF} . Also, $\mathbf{v}_+(\mathbf{k}) = \partial\varepsilon_+/\partial\mathbf{k}$ is the group velocity. In obtaining (28), the left-hand side of the corresponding Eliashberg equations (26a) and (26b) have been averaged over the Fermi surface, $\varepsilon_+(\mathbf{k}) = \nu$. Also, $Z(\mathbf{k}', \omega')$ has been approximated by $Z(\mathbf{k}', \omega)$ on the right-hand side of these equations.

An analysis of the Eliashberg equations (27a), (27b) and of (28) reveals a Lifshitz transition as the interaction $U(\pi)$ grows strong, where the staggered chemical potential ν approaches the upper edge of the band $\varepsilon_+(\mathbf{k})$. In particular, reversing the order of integration in (27a) then yields a divergent wave-function renormalization at the Fermi level [18]:

$$Z(\omega) - 1 = \frac{\varepsilon_E}{\omega}, \quad \text{with} \quad \varepsilon_E = \frac{\pi^2}{4} \epsilon_E. \quad (29)$$

And reversing the order of integration again in (27b) yields the result [18]

$$\nu = \epsilon_E \ln \left(\frac{\omega_{\text{uv}}}{\omega_{\text{ir}}} \right) \ln \left(\frac{W}{\varepsilon_E} \right) \quad (30)$$

for the staggered chemical potential, where ω_{ir} is an infra-red cutoff in the spectrum of hidden spinwaves, and where $W = W_{\text{bottom}} + W_{\text{top}}$ is the electronic bandwidth. Last, assume that the Lifshitz transition leaves ν just below the upper edge of the band $\varepsilon_+(\mathbf{k})$. Figure 5 depicts the later, as well as the new Fermi surface pockets that lie at the corner of the folded (two-iron) Brillouin zone. The Eliashberg energy scale (28) can be easily estimated in the case of small circular Fermi surface pockets as $t_1^{\parallel} \rightarrow 0$. In such case, it is given by [18]

$$\epsilon_E = \frac{1}{16} \left(\frac{x_0}{2\pi} \right)^{3/2} \frac{U^2(\pi)}{a^2 D_+(\nu)} \frac{s_1^2}{a^2 \chi_{\perp}} \frac{|t_2^{\perp}|^2}{(c_0/a) |t_1^{\perp}|^4} \quad (31)$$

in the limit of a small concentration of electrons/holes per pocket, x_0 . Comparison with (30) yields that $x_0 \rightarrow 0$ as $U(\pi) \rightarrow \infty$.

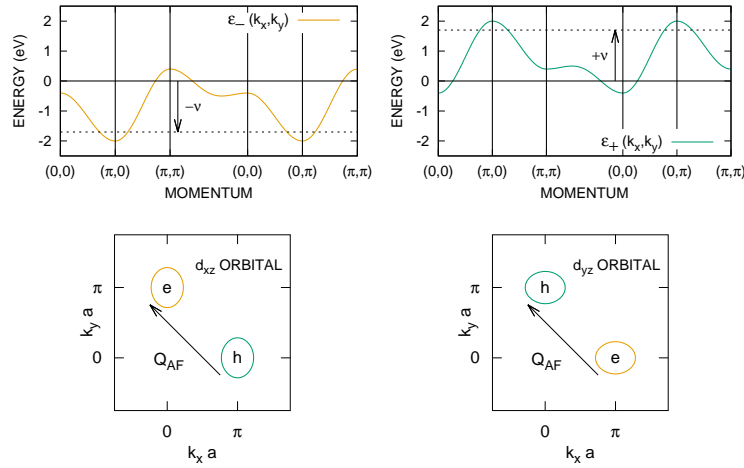


Figure 5. Band structure and renormalized Fermi levels at half filling after the Lifshitz transition. The designated orbital character of the renormalized Fermi surfaces is only approximate.

3.4 Vertex Corrections, Asymptotic Freedom

By Fig. 4a, the previous Eliashberg equations (26a)-(26c) are obtained from the summation of “rainbow” diagrams for the electronic self-energy (21) [44, 45]. Crossing diagrams that lie outside of the previous self-consistent approximation are accounted for by including the correction to the interaction vertex (16) displayed by Fig. 4b. It reads

$$\begin{aligned} \gamma^{(2)}(k, k - \bar{q}') &= i \int_{\text{BZ}} \frac{d^2 k'}{(2\pi)^2} \int_{-\infty}^{+\infty} \frac{dk'_0}{2\pi} \left(\frac{U(\pi)}{\sqrt{2}} \right)^3 \sin[\delta(\mathbf{k}) + \delta(\mathbf{k}')] \sin[\delta(\mathbf{k}' - \mathbf{q}') + \delta(\mathbf{k} - \mathbf{q}')] \\ &\quad \cdot \sin[\delta(\mathbf{k}') + \delta(\mathbf{k}' - \mathbf{q}')] D(k - \bar{k}') \tau_1 G_{\downarrow}(k') \tau_1 G_{\uparrow}(k' - q') \tau_1, \end{aligned} \quad (32)$$

where $\bar{q}' = (q'_0, \mathbf{q}' + \mathbf{Q}_{\text{AF}})$. The integral over frequency can be performed directly, but the calculation is laborious. Instead, we will exploit a Ward identity to perform that integral[46]. In particular, by (19), taking the derivative of the identity $G_{\bar{s}} \cdot G_{\bar{s}}^{-1} = \tau_0$ with respect to $(\text{sgn } s)Z\Delta_0$ yields

$$(\sin 2\delta) G_{\bar{s}} \tau_1 G_{\bar{s}} = -(\text{sgn } s) \frac{\partial G_{\bar{s}}}{\partial (Z\Delta_0)}. \quad (33)$$

Now recall (23) that $G_{\uparrow} = G_{\downarrow}$ at criticality, $Z\Delta_0 \rightarrow 0$. By (21), substituting (33) in for the relevant factors in the integrand on the right-hand side of (32) at $q' = 0$ yields the following Ward identity at criticality[46]:

$$\gamma^{(2)}(k, \bar{k}) = -(\text{sgn } s) \frac{\partial \Sigma_s(k)}{\partial (Z\Delta_0)} \frac{U(\pi)}{\sqrt{2}} \quad \text{as } Z\Delta_0 \rightarrow 0. \quad (34)$$

Approaching criticality, $Z\Delta_0 \rightarrow 0$, comparison of the self-energy correction (20) with the gap equation (26c) yields a correction to the interaction vertex (16) of the form

$$\gamma^{(2)}(k, \bar{k}'') \rightarrow \Gamma^{(2)}(k, \bar{k}'') \frac{U(\pi)}{\sqrt{2}} \sin[\delta(\mathbf{k}) + \delta(\mathbf{k}'')] \tau_1 \quad \text{as } k'' \rightarrow k, \quad (35)$$

with a vertex correction $\Gamma^{(2)}$ equal to minus the kernel of the gap equation: $[1 + \Gamma^{(2)}]Z\Delta_0(\sin 2\delta) = 0$. Expanding the factors of $\sin[\delta(\mathbf{k}) + \delta(\mathbf{k}')] \tau_1$ on the right-hand side of the gap equation (26c) by the standard trigonometric identity reveals the kernel:

$$\begin{aligned} -\Gamma^{(2)}(k, \bar{k}) &= \frac{1}{2} \int_{\text{BZ}} \frac{d^2 k'}{(2\pi)^2} U^2(\pi) \frac{s_1^2 [\sin 2\delta(\mathbf{k}')]^2}{\chi_\perp [Z(\mathbf{k}', \omega')]^2} \frac{1}{E(\mathbf{k}')} \cdot \\ &\cdot \frac{1}{2\omega_b(\mathbf{q})} \left[\frac{1}{\omega_b(\mathbf{q}) + E(\mathbf{k}') - \omega} + \frac{1}{\omega_b(\mathbf{q}) + E(\mathbf{k}') + \omega} \right]. \end{aligned} \quad (36)$$

After substituting $Z(\mathbf{k}', \omega') = \varepsilon_E/E(\mathbf{k}')$ in one of the denominators in the integrand above, then comparison with the second Eliashberg equation (26b) yields the vertex correction at criticality,

$$\Gamma^{(2)} \cong -\frac{1}{2} \frac{\nu}{\varepsilon_E}. \quad (37)$$

Here, the factor $(\varepsilon'_+ - \nu)/Z'E'$ on the right-hand side of (26b) has been set to -1 because $Z'\Delta' = 0$, and because $\nu \rightarrow W_{\text{top}}$ as $U(\pi)$ diverges. Also, the factors of $\sin[\delta(\mathbf{k}) + \delta(\mathbf{k}')] \tau_1$ on the right-hand side of (26b) have been approximated by $\sin[2\delta(\mathbf{k}')] \tau_1$, which is valid because the factor $1/\omega_b(\mathbf{k} - \bar{\mathbf{k}}')$ diverges as $\mathbf{k}' \rightarrow \mathbf{k}$. The vertex correction (37) notably has a negative sign. Also, inspection of the Eliashberg equation (30) yields the solution $\nu/\varepsilon_E \sim \ln(\omega_{\text{uv}}/\omega_{\text{ir}})$.

In the critical hSDW state, the vertex for the interaction of electrons with hidden spinwaves (16) is multiplied by the factor $\Gamma = 1 + \Gamma^{(2)}$ to lowest non-trivial order, with a vertex correction given by (37). Now call $Y = W/\varepsilon_E$. The second Eliashberg equation (30) can then be re-expressed as

$$\ln\left(\frac{\omega_{\text{uv}}}{\omega_{\text{ir}}}\right) = \frac{\nu}{W} \frac{\varepsilon_E}{\varepsilon_E} \frac{Y}{\ln Y}. \quad (38)$$

Here, ω_{uv} and ω_{ir} are the short-range and the long-range cut-offs in wavelength, respectively, for the spectrum of hidden spinwaves. First, by (38), it is important to notice that the Eliashberg energy scale ε_E that controls wavefunction renormalization (29) vanishes logarithmically as $\omega_{\text{ir}} \rightarrow 0$. By Fig. 4b and (37), repeatedly correcting the interaction vertex (16) to lowest non-trivial order then leads to the following renormalization group equation for the strength of the interaction vertex as a function of the ratio of the short-range ultra-violet scale to the long-range infra-red scale:

$$\frac{d\Gamma}{dY} = -\frac{1}{2} \frac{\nu}{W} \Gamma^3. \quad (39)$$

It has the solution

$$Y = \frac{W}{\nu} \frac{1}{\Gamma^2} \quad \text{as } \Gamma \rightarrow 0. \quad (40)$$

Second, (38) thereby yields the renormalization-group flow

$$\ln\left(\frac{\omega_{uv}}{\omega_{ir}}\right) = \frac{\pi^2}{4} \frac{1}{\Gamma^2} \left[\ln\left(\frac{W}{\nu} \frac{1}{\Gamma^2}\right) \right]^{-1} \quad \text{as } \omega_{ir} \rightarrow 0. \quad (41)$$

In conclusion, the present quantum field theory is *asymptotically free* at criticality: $\varepsilon_E \rightarrow 0$ and $\Gamma \rightarrow 0$ as $\ln(\omega_{uv}/\omega_{ir}) \rightarrow \infty$. (Cf. refs. [23], [24], [25] and [26].) If, for example, we impose an $L \times L$ diamond boundary on the square lattice, with periodic boundary conditions for the spin- \uparrow electrons, and with anti-periodic boundary conditions for the spin- \downarrow electrons, then by (16) and (17), $\omega_{ir}/2\pi = c_0/\sqrt{2}L$. The previous therefore implies that spin-flip interactions become weaker and weaker in the critical hSDW state as the size of system approaches the thermodynamic limit.

Last, the previous implies a renormalization-group improved gap equation (26c) for the critical hSDW: $\Gamma Z\Delta_0 \sin(2\delta) = 0$. The flow of the renormalization group (41) correctly yields $Z\Delta_0 = 0$ at $\omega_{ir} > 0$ because $\Gamma > 0$ in such case. However, $\Gamma \rightarrow 0$ as $\omega_{ir} \rightarrow 0$. In other words, the kernel of the gap equation is satisfied as the infra-red wavelength diverges. Such behavior is consisted with assigning the critical hSDW with a quantum critical point.

4 DISCUSSION AND CONCLUSIONS

We have demonstrated above that the quantum-critical hSDW state shows asymptotic freedom: i.e., interactions become weaker and weaker at shorter and shorter length scales compared to that for hidden magnetic order, c_0/ω_{ir} . Under appropriate boundary conditions, the latter is of order the size L of the system. Figure 3b shows a proposed S^{+-} superconducting phase that is controlled by the critical hSDW state[16]. It has only short-range hSDW order[47, 48]. Could the previous renormalization group for asymptotic freedom remain valid there, but with the infra-red length scale c_0/ω_{ir} identified with the finite correlation length for hSDW order instead? If we assume this to be true, then by analogy with the theory of quantum chromodynamics for the strong nuclear force[23, 24, 25, 26], it suggests that the interaction between an electron and a hole in a quantum-disordered groundstate[47, 48] that is close by to the quantum-critical hSDW state (Fig. 3b) is due to a confining string between them. This should occur at separations that are larger than a suitable scale, perhaps equal to the correlation length for hSDW order. Indeed, string states are believed to play a role in the dynamics of the conventional single-orbital Hubbard model over the square lattice, in the context of copper-oxide high-temperature superconductors[27, 28]. It is debated whether confining strings are completely erased by spin-flip interactions, or whether they persist to some degree[29]. We shall now argue that erasing string states by spin-flips is not likely in states with hSDW order.

Figure 6 shows how the propagation of a spin singlet along a principal axis (t_1^{\parallel}) leaves a string of spins that are out of registry with the spin on the opposing orbital per iron atom for SDW and for hSDW order. Notice that strict long-range order is not essential! In the case of the true SDW state on the left-hand side, application of the raising and lowering operators for the net spin at a site, $S_{d+,i}^{\pm} + S_{d-,i}^{\pm}$, can raise or lower the $S_z = 0$ local moments along the string in order to erase it. The string state for the hSDW state shown on the right-hand side of Fig. 6 is not the same, however. It is not possible to erase the string in this case by application of raising and lowering operators for the hidden spin at a site, $S_{d+,i}^{\pm} - S_{d-,i}^{\pm}$, nor is it possible to erase the string by application of the previous raising and lowering operators for the net moment. The previous becomes evident by identifying the ladders of spin states per iron atom that such raising and lowering operators live on. They are shown on the two bottom panels of Fig. 6. Repeated applications of

$S_{d+}^{\pm} + S_{d-}^{\pm}$ and/or of $S_{d+}^{\pm} - S_{d-}^{\pm}$ on the spin $S_z = \pm 1$ moments in the string (red) of the hSDW result in either the opposite moment or in the null state. We therefore conclude that it is unlikely that the string for the hSDW shown in the top-right panel of Fig. 6 can be erased by spin-flip interactions (16).

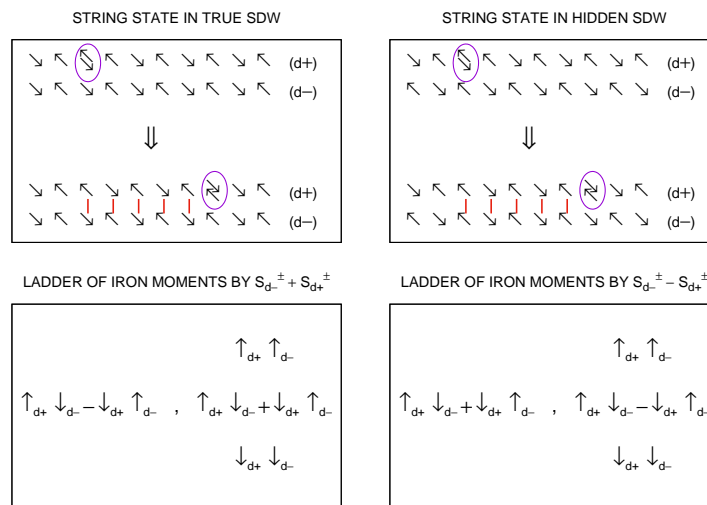


Figure 6. String states in the true SDW and in the hSDW. Also shown are the local irreducible Hilbert spaces that are generated by $S_{d+}^{\pm} + S_{d-}^{\pm}$, as well as the local irreducible Hilbert spaces that are generated by $S_{d+}^{\pm} - S_{d-}^{\pm}$.

In summary, we have shown that a quantum-critical hSDW that is a candidate parent groundstate for electron-doped iron-selenide superconductors shows asymptotic freedom: spin-fluctuation interactions grow weaker and weaker at *relatively* shorter and shorter length scales compared to the size of the system. The critical hSDW state is tuned in by increasing the strength of Hund's Rule until hidden magnetic order is no longer stable [19, 20]. We have suggested that such asymptotic freedom is a symptom of confining string states that appear when a single electron propagates in space and time in the presence of hSDW order. The string picture is therefore consistent with the vanishingly small weight of quasiparticles at the Fermi level at half filling: $1/Z(\omega) = \omega/\varepsilon_F$ as $\omega \rightarrow 0$. In addition, the author has recently shown that electron-doped hSDW states near the critical one studied here show an S^{+-} Cooper pair instability at the Fermi surface [16]. In particular, the pair wavefunction alternates in sign between the electron-type and hole-type Fermi surfaces shown in Fig. 5. However, while the quasi-particle weight of the holes remains vanishingly small at the Fermi level, the quasi-particle weight of the electrons can become appreciable at the Fermi level at sufficient electron doping. Such a dichotomy in the spectral weights between electrons and holes is confirmed by the spectrum of electron-doped hSDW states within a related local-moment model [17]. Within the “quark” picture advocated above, the holes at the hole Fermi surface remain confined and unobservable, while the electrons at the electron Fermi surface are deconfined and observable. This suggests searching for the traces of faint hole bands at the corner of the folded (two-iron) Brillouin zone in electron-doped iron selenide.

CONFLICT OF INTEREST STATEMENT

The author declares that the research was conducted in the absence of any commercial or financial relationships that could be construed as a potential conflict of interest.

FUNDING

This work was supported in part by the US Air Force Office of Scientific Research under grant no. FA9550-17-1-0312.

ACKNOWLEDGMENTS

The author thanks Alex Kass, Ronald Melendrez, Geovani Montoya, and Tong Wang for helpful discussions.

REFERENCES

- [1] S. He, J. He, W.-H. Zhang, L. Zhao, D. Liu, X. Liu, D. Mou, Y.-B. Ou, Q.-Y. Wang, Z. Li, L. Wang, Y. Peng, Y. Liu, C. Chen, L. Yu, G. Liu, X. Dong, J. Xiang, C. Chen, Z. Xu, X. Chen, X. Ma, Q. Xue, and X.J. Zhou, “Phase Diagram and Electronic Indication of High-Temperature Superconductivity at 65 K in Single-Layer FeSe Films”, *Nat. Mater.* **12**, 605 (2013).
- [2] W.-H. Zhang, Y. Sun, J.-S. Zhang, F.-S. Li, M.-H. Guo, Y.-F. Zhao, H.-M. Zhang, J.-P. Peng, Y. Xing, H.-C. Wang, T. Fujita, A. Hirata, Z. Li, H. Ding, C.-J. Tang, M. Wang, Q.-Y. Wang, K. He, S.-H. Ji, X. Chen, J.-F. Wang, Z.-C. Xia, L. Li, Y.-Y. Wang, J. Wang, L.-L. Wang, M.-W. Chen, Q.-K. Xue, and X.-C. Ma, “Direct Observation of High-Temperature Superconductivity in One-Unit-Cell FeSe Films”, *Chin. Phys. Lett.* **31**, 017401 (2014).
- [3] T. Qian, X.-P. Wang, W.-C. Jin, P. Zhang, P. Richard, G. Xu, X. Dai, Z. Fang, J.-G. Guo, X.-L. Chen, H. Ding, “Absence of a Holelike Fermi Surface for the Iron-Based $K_{0.8}Fe_{1.7}Se_2$ Superconductor Revealed by Angle-Resolved Photoemission Spectroscopy”, *Phys. Rev. Lett.* **106**, 187001 (2011).
- [4] R. Peng, X.P. Shen, X. Xie, H.C. Xu, S.Y. Tan, M. Xia, T. Zhang, H.Y. Cao, X.G. Gong, J.P. Hu, B.P. Xie, D. L. Feng, “Measurement of an Enhanced Superconducting Phase and a Pronounced Anisotropy of the Energy Gap of a Strained FeSe Single Layer in FeSe/Nb: $SrTiO_3/KTaO_3$ Heterostructures Using Photoemission Spectroscopy”, *Phys. Rev. Lett.* **112**, 107001 (2014).
- [5] J.J. Lee, F.T. Schmitt, R.G. Moore, S. Johnston, Y.-T. Cui, W. Li, M. Yi, Z.K. Liu, M. Hashimoto, Y. Zhang, D.H. Lu, T.P. Devereaux, D.-H. Lee and Z.-X. Shen, “Interfacial Mode Coupling as the Origin of the Enhancement of T_c in FeSe Films on $SrTiO_3$ ”, *Nature* **515**, 245 (2014).
- [6] L. Zhao, A. Liang, D. Yuan, Y. Hu, D. Liu, J. Huang, S. He, B. Shen, Y. Xu, X. Liu, L. Yu, G. Liu, H. Zhou, Y. Huang, X. Dong, F. Zhou, Z. Zhao, C. Chen, Z. Xu and X.J. Zhou, “Common Electronic Origin of Superconductivity in $(Li,Fe)OHFeSe$ Bulk Superconductor and Single-Layer FeSe/ $SrTiO_3$ Films”, *Nat. Comm.* **7**, 10608 (2016).
- [7] Q. Fan, W.H. Zhang, X. Liu, Y.J. Yan, M.Q. Ren, R. Peng, H.C. Xu, B.P. Xie, J.P. Hu, T. Zhang, and D.L. Feng, “Plain S-Wave Superconductivity in Single-Layer FeSe on $SrTiO_3$ Probed by Scanning Tunneling Microscopy”, *Nat. Phys.* **11**, 946 (2015).
- [8] Y.J. Yan, W.H. Zhang, M.Q. Ren, X. Liu, X.F. Lu, N. Z. Wang, X.H. Niu, Q. Fan, J. Miao, R. Tao, B.P. Xie, X.H. Chen, T. Zhang, D.L. Feng, “Surface Electronic Structure and Evidence of Plain S-Wave Superconductivity in $(Li_{0.8}Fe_{0.2})OHFeSe$ ”, *Phys. Rev. B* **94**, 134502 (2016).
- [9] I.I. Mazin, D.J. Singh, M.D. Johannes, and M.H. Du, “Unconventional Superconductivity with a Sign Reversal in the Order Parameter of $LaFeAsO_{1-x}F_x$ ”, *Phys. Rev. Lett.* **101**, 057003 (2008).
- [10] K. Kuroki, S. Onari, R. Arita, H. Usui, Y. Tanaka, H. Kontani, and H. Aoki, “Unconventional Pairing Originating from the Disconnected Fermi Surfaces of Superconducting $LaFeAsO_{1-x}F_x$ ”, *Phys. Rev. Lett.* **101**, 087004 (2008).
- [11] J.T. Park, G. Friemel, Yuan Li, J.-H. Kim, V. Tsurkan, J. Deisenhofer, H.-A. Krug von Nidda, A. Loidl, A. Ivanov, B. Keimer, and D. S. Inosov, “Magnetic Resonant Mode in the Low-Energy Spin-Excitation Spectrum of Superconducting $Rb_2Fe_4Se_5$ Single Crystals”, *Phys. Rev. Lett.* **107**, 177005 (2011).
- [12] G. Friemel, J.T. Park, T. A. Maier, V. Tsurkan, Yuan Li, J. Deisenhofer, H.-A. Krug von Nidda, A. Loidl, A. Ivanov, B. Keimer, and D.S. Inosov, “Reciprocal-Space Structure and Dispersion of the Magnetic Resonant Mode in the Superconducting Phase of $Rb_xFe_{2-y}Se_2$ Single Crystals”, *Phys. Rev. B* **85**, 140511(R) (2012).

- [13] N.R. Davies, M.C. Rahn, H.C. Walker, R.A. Ewings, D.N. Woodruff, S.J. Clarke, and A.T. Boothroyd, “Spin Resonance in the Superconducting State of $\text{Li}_{1-x}\text{Fe}_x\text{ODFe}_{1-y}\text{Se}$ Observed by Neutron Spectroscopy”, *Phys. Rev. B* **94**, 144503 (2016).
- [14] M. Ma, L. Wang, P. Bourges, Y. Sidis, S. Danilkin, and Y. Li, “Low-energy Spin Excitations in $(\text{Li}_{0.8}\text{Fe}_{0.2})\text{ODFeSe}$ Superconductor Studied with Inelastic Neutron Scattering”, *Phys. Rev. B* **95**, 100504(R) (2017).
- [15] B. Pan, Y. Shen, D. Hu, Y. Feng, J.T. Park, A.D. Christianson, Q. Wang, Y. Hao, H. Wo, Z. Yin, T.A. Maier and J. Zhao, “Structure of Spin Excitations in Heavily Electron-Doped $\text{Li}_{0.8}\text{Fe}_{0.2}\text{ODFeSe}$ Superconductors”, *Nat. Comm.* **8**, 123 (2017).
- [16] J.P. Rodriguez, “Superconductivity by Hidden Spin Fluctuations in Electron-Doped Iron Selenide”, arXiv:2001.07908 .
- [17] J.P. Rodriguez, “Isotropic Cooper Pairs with Emergent Sign Changes in a Single-Layer Iron Superconductor”, *Phys. Rev. B* **95**, 134511 (2017).
- [18] J.P. Rodriguez and R. Melendrez, “Fermi Surface Pockets in Electron-Doped Iron Superconductor by Lifshitz Transition”, *J. Phys. Commun.* **2**, 105011 (2018); “Corrigendum: Fermi Surface Pockets in Electron-Doped Iron Superconductor by Lifshitz Transition”, *J. Phys. Commun.* **3**, 019501 (2019).
- [19] J.P. Rodriguez and E.H. Rezayi, “Low Ordered Magnetic Moment by Off-Diagonal Frustration in Undoped Parent Compounds to Iron-Based High- T_c Superconductors”, *Phys. Rev. Lett.* **103**, 097204 (2009).
- [20] J.P. Rodriguez, “Magnetic Excitations in Ferropnictide Materials Controlled by a Quantum Critical Point into Hidden Order”, *Phys. Rev. B* **82**, 014505 (2010).
- [21] J.R. Rodriguez, “Spin Resonances in Iron-Selenide High- T_c Superconductors by Proximity to Hidden Spin Density Wave”, arXiv:2002.01732 .
- [22] E. Berg, M.A. Metlitski, and S. Sachdev, “Sign-Problem-Free Quantum Monte Carlo of the Onset of Antiferromagnetism in Metals”, *Science* **338**, 1606 (2012).
- [23] H.D. Politzer, “Reliable Perturbative Results for Strong Interactions?”, *Phys. Rev. Lett.* **30**, 1346 (1973).
- [24] D.J. Gross and F. Wilczek, “Ultraviolet Behavior of Non-Abelian Gauge Theories”, *Phys. Rev. Lett* **30**, 1343 (1973).
- [25] Pierre Ramond, *Field Theory. A Modern Primer* (Benkamin Cummings, Reading, 1981).
- [26] A.M. Polyakov, *Gauge Fields and Strings* (Harwood Academic Publishers, London, 1987).
- [27] S.A. Trugman, “Interaction of Holes in a Hubbard Antiferromagnet and High-Temperature Superconductivity”, *Phys. Rev. B* **37**, 1597 (1988).
- [28] B.I. Shraiman and E.D. Siggia, “Mobile Vacancies in a Quantum Heisenberg Antiferromagnet”, *Phys. Rev. Lett.* **61**, 467 (1988).
- [29] E. Dagotto, “Correlated Electrons in High-Temperature Superconductors”, *Rev. Mod. Phys.* **66**, 763 (1994).
- [30] S. Raghu, Xiao-Liang Qi, Chao-Xing Liu, D.J. Scalapino, Shou-Cheng Zhang, “Minimal Two-Band Model of the Superconducting Iron Oxypnictides”, *Phys. Rev. B* **77**, 220503(R) (2008).
- [31] P.A. Lee and X.-G. Wen, “Spin-Triplet P-Wave Pairing in a Three-Orbital Model for Iron Pnictide Superconductors”, *Phys. Rev. B* **78**, 144517 (2008).
- [32] J.P. Rodriguez, M.A.N. Araujo and P.D. Sacramento, “Emergent Nesting of the Fermi Surface from Local-Moment Description of Iron-Pnictide High- T_c Superconductors”, *Eur. Phys. J. B* **87**, 163 (2014).
- [33] M. Daghofer, A. Moreo, J.A. Riera, E. Arrigoni, D.J. Scalapino, and E. Dagotto, “Model for the Magnetic Order and Pairing Channels in Fe Pnictide Superconductors”, *Phys. Rev. Lett.* **101**, 237004

- (2008); A. Moreo, M. Daghofer, J.A. Riera, and E. Dagotto, “Properties of a Two-Orbital Model for Oxypnictide Superconductors: Magnetic Order, B_{2g} Spin-Singlet Pairing Channel, and its Nodal Structure”, Phys. Rev. B **79**, 134502 (2009).
- [34] P.W. Anderson, “Antiferromagnetism. Theory of Superexchange Interaction”, Phys. Rev. **79**, 350 (1950).
- [35] Q. Si and E. Abrahams, “Strong Correlations and Magnetic Frustration in the High- T_c Iron Pnictides”, Phys. Rev. Lett. **101**, 076401 (2008).
- [36] J.E. Hirsch, “Two-Dimensional Hubbard Model: Numerical Simulation Study”, Phys. Rev. **B 31**, 4403 (1985).
- [37] S. Nandi, M. G. Kim, A. Kreyssig, R. M. Fernandes, D. K. Pratt, A. Thaler, N. Ni, S. L. Bud’ko, P. C. Canfield, J. Schmalian, R. J. McQueeney, and A. I. Goldman, Phys. Rev. Lett. **104**, 057006 (2010).
- [38] M. Yoshizawa and S. Simayi, “Anomalous Elastic Behavior and its Correlation with Superconductivity in Iron-Based Superconductor $\text{Ba}(\text{Fe}_{1-x}\text{Co}_x)_2\text{As}_2$ ”, Mod. Phys. Lett. B **26**, 1230011 (2012).
- [39] P.W. Anderson, “An Approximate Quantum Theory of the Antiferromagnetic Ground State”, Phys. Rev. **86**, 694 (1952).
- [40] B. I. Halperin and P. C. Hohenberg, “Hydrodynamic Theory of Spin Waves”, Phys. Rev. **188**, 898 (1969).
- [41] D. Forster, *Hydrodynamic Fluctuations, Broken Symmetry, and Correlation Functions* (Benjamin/Cummings, Reading, MA, 1975).
- [42] Y. Nambu, “Quasi-Particles and Gauge Invariance in the Theory of Superconductivity”, Phys. Rev. **117**, 648 (1960).
- [43] L.P. Gorkov, Zh. Eksperim. i Teor. Fiz. **34**, 735 (1958); “About the Energy Spectrum of Superconductors”, Sov. Phys. JETP **7**, 505 (1958).
- [44] J.R. Schrieffer, *Theory of Superconductivity* (Benjamin, New York, 1964).
- [45] D.J. Scalapino, in R.D. Parks (ed.) *Superconductivity*, vol. I (Dekker, New York, 1969).
- [46] J.C. Ward, Phys. Rev. **78**, 182 (1950).
- [47] S. Chakravarty, B.I. Halperin, and D.R. Nelson, “Two-Dimensional quantum Heisenberg Antiferromagnet at Low Temperatures”, Phys. Rev. B **39**, 2344 (1989).
- [48] J.P. Rodriguez, “Effect of Topological Excitations in the Two-Dimensional Quantum Heisenberg Antiferromagnet”, Phys. Rev. **41**, 7326(R) (1990).